Materials Chemistry and Physics 240 (2020) 122163

Contents lists available at ScienceDirect

Materials Chemistry and Physics

journal homepage: www.elsevier.com/locate/matchemphys

Synthesis of molybdenum oxide nanoparticles by nanosecond laser ablation

Noe Zamora-Romero [a], Miguel A. Camacho-Lopez [b,*], Alfredo R. Vilchis-Nestor [c], Victor H. Castrejon-Sanchez [d], Guillermo Aguilar [e], Santiago Camacho-Lopez [f], Marco Camacho-Lopez [g,**]

[a] University of California, Riverside, Department of Materials Science and Engineering, 900 University Avenue, Riverside, CA, 92521, United States
[b] Laboratorio de Fotomedicina, Biofotónica y Espectroscopía Láser de Pulsos Ultracortos, Facultad de Medicina, Universidad Autónoma del Estado de México, Jesús Carranza y Paseo Tollocan s/n, Toluca, 50120, Mexico
[c] Centro Conjunto de Investigación en Química Sustentable, UAEM-UNAM. Facultad de Química. Universidad Autónoma del Estado de México, Toluca, 50120, Mexico
[d] Tecnologico de Estudios Superiores de Jocotitlan, Carretera Toluca Atlacomulco Km 44.8, Ejido San Juan y San Agustin, Jocotitlan, 50700, Mexico
[e] University of California, Riverside, Department of Mechanical Engineering, 900 University Avenue, Riverside, CA, 92521, United States
[f] Centro de Investigación Científica y de Educación Superior de Ensenada, Carretera Ensenada-Tijuana, No. 3918, Zona Playitas, Ensenada, B.C, 22860, Mexico
[g] Laboratorio de Investigación y Desarrollo de Materiales Avanzados, Facultad de Química, Universidad Autónoma del Estado de México, Campus Rosedal, Km 14.5 Carretera Toluca-Atlacomulco, Toluca, 50925, Mexico

HIGHLIGHTS

- MoOx NPs were successfully synthesized by the LASL method with ns pulses.
- MoOx NPs possess an absorption peak located at around 840 nm.
- The produced MoOx NPs show potential for Photothermal Theraphy applications.
- MoOx NPs are constituted of amorphous molybdenum oxide hydrates ($MoO_3 \cdot xH_2O$).

ARTICLE INFO

Keywords:
Photothermal therapy
Photothermal agent
Molybdenum oxide
Laser ablation
Nanoparticles fragmentation

ABSTRACT

Photothermal therapy (PTT) is one of the most promising techniques to treat cancer. Finding the ideal PTT agent nanomaterial has remained a challenge and has brought the interest of several researchers. In this work, we report the synthesis of molybdenum oxide (MoO_x) nanoparticles (NPs), which exhibit absorption in the biological optical window ~840 nm, by using the laser ablation of solids in liquids (LASL) technique with nanosecond (ns) pulses. A Nd:YAG laser was used to synthesize the NPs in deionized (DI) water, free of surfactants or additives, which were optically characterized by absorption spectroscopy and TEM-EDX microscopy. Semi spherical NPs with a suitable average size and shape for potential use as PTT agents were obtained by laser ablation and ablation + fragmentation. The calculated band gap is 3.1 eV, which corresponds to MoO_3. Micro-Raman spectroscopy studies determined that these NPs are composed of amorphous molybdenum oxide hydrates ($MoO_3 \cdot xH_2O$).

1. Introduction

PTT has shown remarkable results for selective tumor ablation, some of the advantages of this therapy are that it is noninvasive and relatively easy to perform [1–4]. Finding the most suitable PTT agent is essential for the progress and possible implementation of this therapy in clinical trials, nevertheless it has been and still a challenge for researchers because of the peculiar properties a PTT agent must possess. Noble nanomaterials have been the most explored so far, especially the ones made of Au [5–8]. However, its practical application is limited by their high cost, and other materials are being considered [9–11].

In recent years one of the most attractive materials for a wide range of potential applications, ranging from optical and electronic to energy and bio devices is MoO_x [12–24]. Some of these oxides exhibit surface

* Corresponding author.
** Corresponding author.
E-mail addresses: macamachol@uaemex.mx (M.A. Camacho-Lopez), camachol@cicese.mx (S. Camacho-Lopez).

https://doi.org/10.1016/j.matchemphys.2019.122163
Received 12 June 2019; Received in revised form 3 September 2019; Accepted 10 September 2019
Available online 11 September 2019

plasmon resonance (SPR) across different spectral regions; this enables optical tunability, which permits the synthesis of nanostructures (NS) that absorb light in the near infrared (NIR), where light has the deepest penetration in biotissue [17–24]. In fact, different MoO_x NS have been used as PTT agents with very promising results, since these materials have shown low toxicity, strong NIR absorption and photothermal conversion efficiency [20–24].

Different groups have synthesized MoO_x NS using chemical synthesis methods. For instance, Yin, et al., reported PEG-MoO_x NPs that exhibit broad absorption in the NIR region and strong photothermal conversion ability, they showed these NPs can be used to treat tumors by synergetic PTT and photodynamic therapy (PDT) in *vitro* experiments [21]. Liu et al., obtained chemical highly stable MoO_2 bow tie-like NPs by using a hydrothermal method as well, and showed they could withstand high temperature heating without oxidation and have a SPR effect from visible to NIR [22].

Furthermore, Zhan, et al., synthesized low cost and stable MoO_2 NPs with tunable phase by using a solvothermal method and found that the photothermal conversion efficiency as high as 61.3%, this was attributed to the large amount of free electrons provided by the sufficient concentration of oxygen vacancies [23]. Besides, Song, et al., generated hydrophilic molybdenum trioxide MoO_3-Poly-ethylene-glycol (PEG) nanospheres and nanoribbons by using a hydrothermal method and reported these NS to have a strong SPR in the NIR region and can be used in hyperthermia therapy [24].

On the other hand, the LASL method has shown to be successful for synthesizing a big variety of NS [25–33], including MoO_x NS [30–33]. Some of the advantages of this technique are that it is a straightforward, one-step and clean synthesis method, since it produces reduced or nonexistent byproducts and there is no need for catalyst. These NS are generated in ambient conditions, not extreme temperature or pressure are needed and some properties of the synthesized NS (shape, size distribution) can be conveniently controlled upon LASL by conveniently adjusting the laser parameters or changing the type of liquid medium [35,36].

In Ref. [30], core shell-type MoO_x NS with average sizes from 48 to 141 nm were synthesized by picosecond LASL. The absorption spectra of the colloidal solution shows a peak around 210 nm and a shoulder around 240 nm. An oxidation process of the NS due to aging was proposed. In Ref. [31], nickel-molybdenum alloys were generated by ns LASL. An absorption peak at about 215 nm and a shoulder at 240 nm, which correspond to MoO_3 NPs was found. It was also reported that after few weeks two absorption bands appeared from 500 to 900 nm.

However, in spite of the great potential application of the MoO_x NS as PTT agents in one hand, and the versatility and popularity of LASL one the other, this type of NS have never been synthesized with these properties with ns pulses as far as we know. This is the motivation of our present work, where we report on the generation of MoO_x by the LASL method.

The NPs obtained are free of surfactants or additives and exhibit absorbance in the so called optical biological window around 840 nm, which makes them suitable as PTT agents. They were obtained by ablating a Mo target submerged in deionized water, with a ns laser for either 30 min or 20 min plus 10 more of colloidal irradiation; the last was performed with the purpose of studying NPs fragmentation. TEM-EDX scans images show molybdenum and oxygen distribution in the NS, and the band gap was calculated by using Tauc's rule with values of 3.1 eV. Micro-Raman studies indicate these NPs are composed of molybdenum trioxide hydrates ($MoO_3 \cdot xH_2O$).

2. Experimental

2.1. Synthesis of the Mo NPs colloidal suspensions

A nanosecond (ns) Nd:YAG (continuum minilite) pulsed laser and a highly pure (99.95%) Mo target disk (*Kurt J, Lesker Co*) with a 7 mm depth were used to synthesize the NPs. The target was submerged in 6 ml of DI water, forming a 1 cm height column from the surface. Then it was irradiated with a beam of 25 mJ, focused with a 200 mm focal lens forming a 27.5 μm diameter beam on the material surface. The per pulse laser energy and laser repetition rate frequency were kept constant. The experiments were performed at room temperature with not external extreme temperature or pressure were needed. (Fig. 1).

To study the effect of fragmentation on the NPs properties, two experiments were carried out. The idea was to keep all parameters constant but the time of target irradiation. In the first one, the target was continuously ablated for 30 min. In the second one, the same target was ablated for 20 min, then it was taken out of the container and the generated colloidal solution was irradiated for 10 min to induce fragmentation. The pulse length was 7 ns and its fluence was 4.2 J/cm^2, the laser pulses were delivered at 10 Hz and a wavelength of 1064 nm. The Mo target was rotating while ablating in order to avoid irradiation of the same target spot.

2.2. Sample characterization

2.2.1. UV–Vis characterization

A double beam spectrometer (Lambda 650 from Perkin-Elmer) with range scanning from 200 to 900 nm was utilized to carry out the optical characterization of the obtained colloidal suspensions. A quartz cuvette with an optical path length of 10 mm was used, the optical absorption spectra measurements were taken three days after the NPs synthesis.

2.2.2. TEM-EDX

The morphology, size and structure studies of the Mo NPs were performed on a Transmission Electron Microscope-EDX (JEM 2100 from JEOL) operated at 120 kV accelerating voltage equipped with a LaB_6 filament. For sample preparation, a drop of the NPs suspension was placed on a lacey-carbon Cu grid, it was allow to evaporate at room conditions and then was observed in the TEM. In order to obtain information of the particle size and distribution, the dimensions of many particles were measured employing the ImageJ™ software.

2.2.3. Raman micro-spectroscopy

Raman spectra were recorded by using a micro-Raman Horiba Jobin Yvon system, model Xplora plus. A solid-state laser at 532 nm with a nominal power of 25 mW was used to generate the Raman signal. A 100x objective lens was used to focus the laser beam and also served the purpose of collecting the scattered light. The delivered laser power on the sample surface was 1% of the nominal power. A 1200 lines/mm grating was employed, 100 acquisitions were averaged with an exposure

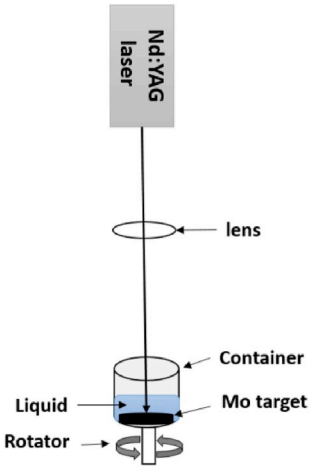

Fig. 1. Schematic of the LASL experimental set up used to synthesize the MoO_X NPs.

time of 1 s each one.

3. Results and discussion

3.1. Optical properties of Mo NPs colloidal suspensions

Fig. 2 shows the absorbance of the colloidal solutions in DI water obtained by ablating the target with 4.2 J/cm^2 for 30 min and 20 min plus 10 min of irradiation. It can be seen on both spectra that the value of the absorbance is relatively high for wavelengths below 400 nm, this is related to metallic Mo NPs [37]. There is a peak at around 840 nm, which is attributed to the formation of MoO_x NPs in this size range -tenths of nanometers- similar spectra have been obtained for MoO_x NPs with similar diameters by chemical methods [21].

Moreover, even though both spectra look very similar, there are two subtle but important differences. On the one hand, the value of the absorbance is clearly higher for the colloidal solution obtained with 30 min of constant ablation (black squares), this is due to the fact that the solution is more concentrated since longer times of ablation produce a larger amount of NPs [34–36].

On the other hand, the absorbance peak for the colloidal solution obtained with 20 min of ablation plus 10 min of irradiation (red triangles) is slightly red shifted respect to the one obtained for 30 min of continues ablation (black squares), it is located at 844 nm. The last is explained by NPs fragmentation produced by the extra irradiation time of the colloidal solution. It is well-known from the Mie scattering theory that the optical properties of nanostructures are directly related to its size [38].

Having NPs that exhibit an absorption peak in the NIR range is mandatory for the purpose of using them as PTT agents. NIR light penetrates deep in biotissue, this is why finding an absorbance peak at around 840 nm in this work is remarkable, especially because it has never been reported when synthesizing MoO_x NPs with suitable sizes for PTT by LASL with ns pulses. Another significant result is demonstrating the NPs synthesis free of surfactants, additives or any chemical pollutant as opposite to most chemical methods [21–24].

3.2. Band gap estimation

In order to estimate the energy band gap of the NS synthesized, the data from UV–Vis absorption and Tauc's rule were used [39,40].

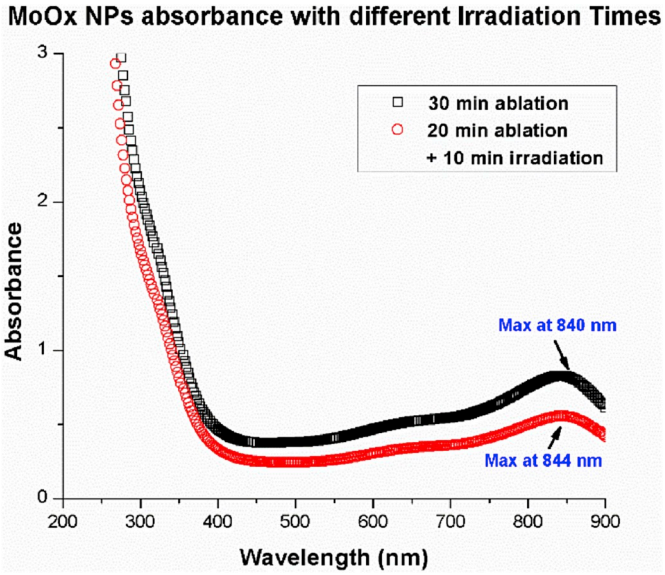

Fig. 2. MoO_x NPs colloidal suspension absorbance spectra.

$$(\alpha h\nu)^{1/n} \approx (h\nu - E_g)$$

where α is the absorption coefficient, h is Plank's constant, ν is the frequency of photon, E_g is the energy band gap and the $n = ½$ for a direct band gap [41–43].

The band gap energy results are shown in Fig. 3. The estimated value obtained is 3.1 eV for both colloidal solutions generated either (a) with 30 min of continuous ablation or (b) 20 min ablation +10 min colloidal irradiation, respectively, which correspond to the semiconductor MoO_3 [12].

3.3. TEM images of the Mo NPs

Representative TEM micrographs of the MoO_x NPs obtained and corresponding size distribution graphs for the two experiments are shown in Fig. 4. Fig. 4(a), 4(b) and 4(c) shows images corresponding to the continuous ablation of the Mo target for 30 min. Figure 4(a) shows core-shell type NPs with sizes from 20 and up to 100 nm; particularly in the largest one, marked with arrows it can be seen that the Mo core looks darker, since it is denser than the MoO_x shell that surrounds it, which looks light grey [29]. In figure 4(b) semi spherical NPs with various sizes are seen in a different scale, these NPs were obtained under the same laser irradiation parameters. The graph in Fig. 4(c) shows that the size range spans from 6.5 to 100.3 nm and it has a bimodal size distribution with peaks at 25 nm and 90 nm.

Fig. 4(d) show representative images of the MoO_x NPs obtained with 20 min of ablation plus 10 min of colloidal solution irradiation. In Fig. 4 (e), we can see semispherical core-shell type NPs of various sizes in a different scale, obtained under the same laser irradiation parameters. Finally, the graph in Fig. 4(f) shows that the size range spans from 7 to 52 nm and it also has a bimodal size distribution with peaks at 16 and 28 nm.

During laser irradiation of the colloidal solution, NPs absorbed energy and their temperature promptly approaches the melting point, which causes them to fragment [44]. The effect of inducing NPs fragmentation, by irradiating the colloidal solution after removing the target, is clearly seen when comparing the size distribution of the two samples. For instance, it can be seen that the size peak of fig. 4(c) is 25 nm compared to 16 nm, in Fig. 4(f), correspondingly the second peak is around 90 nm whereas in the latter is reduced to 28 nm. A plausible explanation for this is that the absorption coefficient is larger for larger NPs [44].

These size reduction was expected and it is in agreement with other reports for other materials synthesized by LASL with similar irradiation parameters. Obtaining a bimodal size distribution is common when synthesizing NS with ns pulses and the two possible responsible explanations for this are thermal vaporization and explosive intensity boiling [26,35,36].

3.4. TEM-EDX images of the Mo NPs

The elemental distribution of the NS generated was studied by using TEM-EDX images and two elements were found. Fig. 5 shows representative EDX line scans images, it can be seen in both NPs scanned that they are composed mainly of molybdenum and some oxygen, and the elemental distribution may correspond to a core-shell type NS [45,46], in which the core is made of metallic molybdenum shown with a blue line in the spectra, and it is surrounded by molybdenum oxide which corresponds to the superposition of blue and green lines in the spectra, as proposed in Ref. [30].

3.5. Raman spectroscopy

The formation of oxides may be generated when ablated species react with dissolved molecular or water bound oxygen deliberated

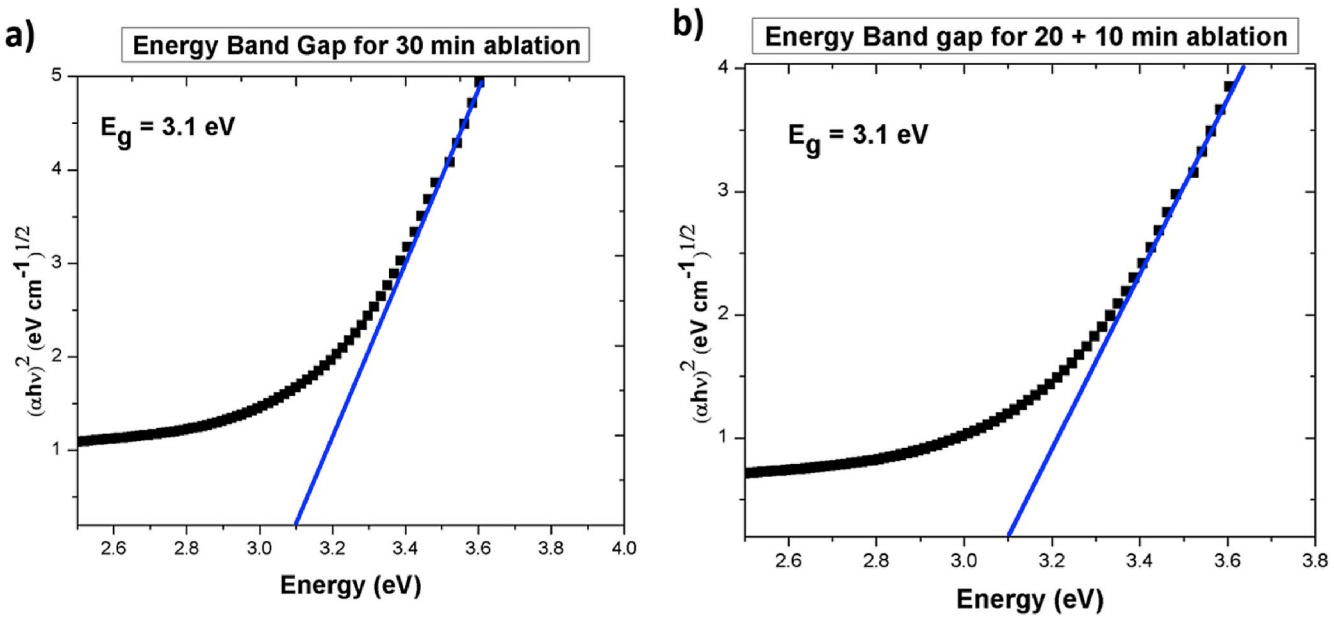

Fig. 3. Energy band gap calculation for the colloidal solutions by using Tauc's method for (a) 30 min ablation and (b) 20 min ablation +10 min of colloidal irradiation.

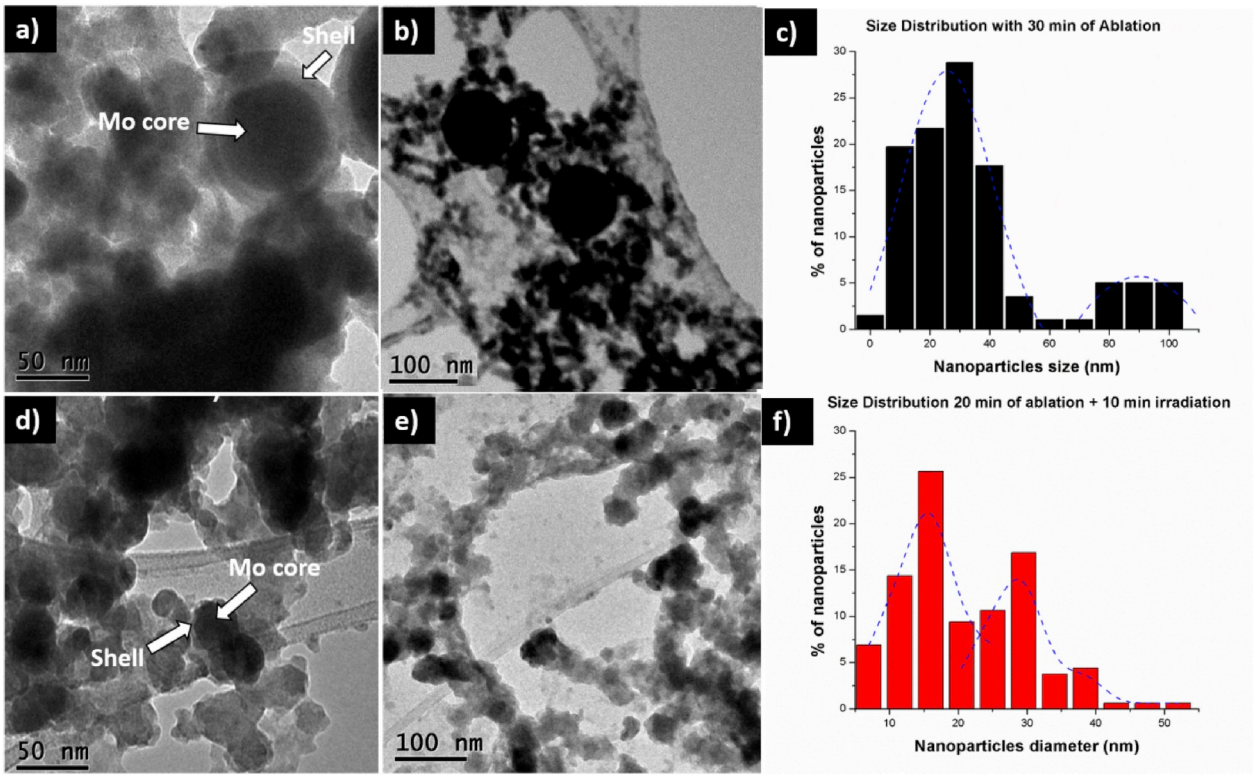

Fig. 4. TEM images of MoO_X NPs obtained and their corresponding size distribution graphs when ablating the Mo target for 30 min continuously in figure (a), (b) and (c), and for 20 min plus 10 min of irradiation of the colloidal solution in (d), (e) and (f).

simultaneously by the photothermal decomposition of the water when plasma is cooling [31]. The obtained Raman spectrum for the samples irradiated for 30 min is shown in Fig. 6, the one obtained for 20 min ablation plus 10 min of colloidal irradiation was almost identical and for space reasons it is not shown.

The different bands are associated with molybdenum oxide hydrates ($MoO_3{\cdot}H_2O$) [47–49]. These compounds structure comes from the presence of MoO_5 (OH_2) octahedral, sharing either corner equatorial oxygens or edges that exhibit different vibration modes. A broad band can be seen in the left part of the spectrum from 297 to 460 cm^{-1}, which might correspond to several νMo-OH_2 vibrations, coming from several Mo–H_2O distances and/or dipolar coupling between several of such oscillations. A weak signal at 520 cm^{-1} can be identified, which is related to the stretching vibration of O–Mo_3 units.

In the right part of the spectrum, there are two strong signals. The first peak at 810 cm^{-1} might come from the stretching vibrations of

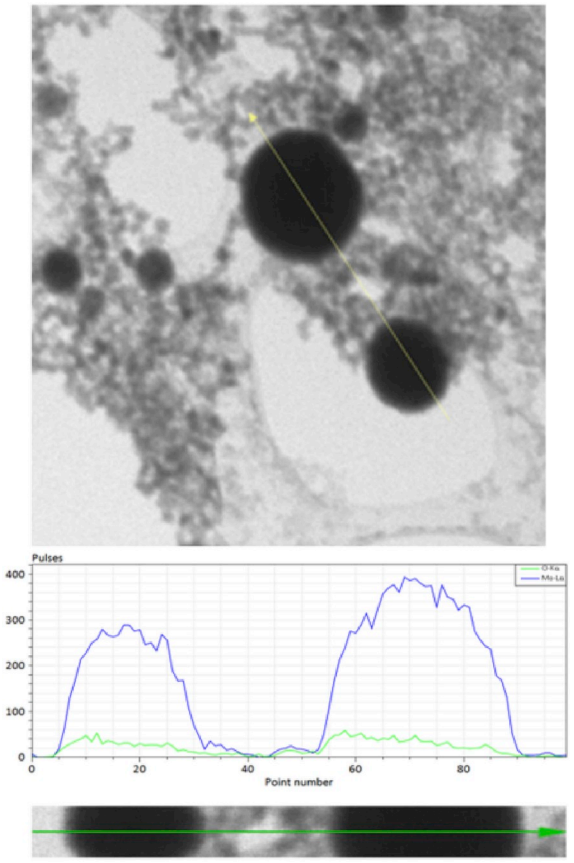

Fig. 5. TEM-EDX images of MoO_X NPs obtained with 30 min of continues ablation.

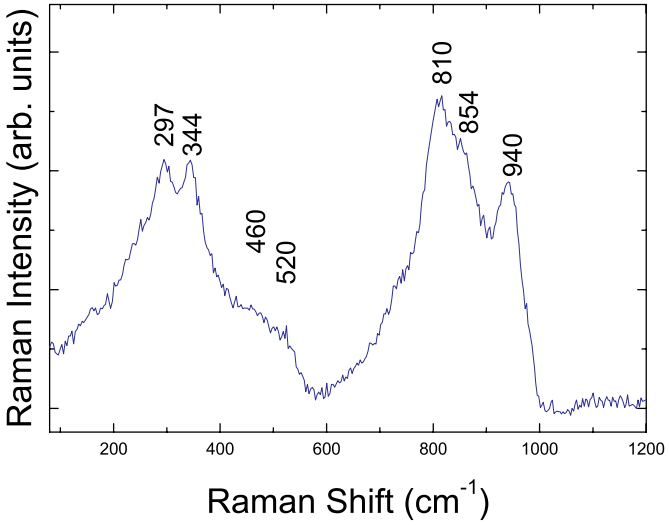

Fig. 6. Raman spectrum of the obtained hydrated molybdenum trioxide.

Mo_3–O–Mo_3 units, which is related to α-MoO_3. The second peak at 854 cm^{-1} is located in a spectral range where stretching vibrations are associated to Mo–O bonds corresponding to β-MoO_3. Finally, there is a broad peak at 940 cm^{-1} which is described as the νOH = Mo stretching vibration unit [47–49].

4. Conclusions

This work reports the generation of MoO_x NPs by using the LASL method with ns laser pulses. The produced NPs show potential as PTT agents. The synthesis of these NPs is surfactants/additives free. Remarkably, these MoO_x NPs possess an absorption peak in the optical biological window, this peak is located at around 840 nm and size peaks from 16 to 90 nm, which makes them suitable for PTT. The TEM-EDX images show the elemental composition and distribution and bimodal sizes with peaks at 25 and 90 nm, and 16 and 28 nm for ablation of 30 min and 20 min ablation +10 min of colloidal irradiation, respectively. As a result of the NPs laser-induced fragmentation the NPs size decreases. As a consequence the absorption peak is red shifted and the calculated energy band gap is 3.1 eV, which corresponds to MoO_3. Micro-Raman study shows this NS are constituted of amorphous molybdenum oxide hydrates ($MoO_3 \cdot xH_2O$). Future research is being conducted to set the irradiation parameters for optimizing the NPs absorbance in the NIR range and carry out hyperthermia studies with cw irradiation.

Conflicts of interest

All authors claim not to have conflict of interest related to this article.

Acknowledgments

This work was possible thanks to the UCMEXUS-CONACYT scholarship for doctoral studies awarded to Noe Zamora-Romero. TEM facilities were financial supported by CONACYT-Mexico (Grant No. 280518).

References

[1] D.P. O'Neal, L.R. Hirsch, N.J. Halas, J.D. Payne, J.L. West, Photo-thermal ablation in mice using near infrared-absorbing nanoparticles, Cancer Lett. 209 (2004) 171–176. https://doi.org/10.1016/j.canlet.2004.02.004.

[2] I.H. El-Sayed, X. Huang, M.A. El-Sayed, Selective laser photo-thermal therapy of epithelial carninoma using anti-EFGR antibody conjugated gold nanoparticles, Cancer Lett. 239 (2006) 129–135. https://doi.org/10.1016/j.canlet.2005.07.035.

[3] C. Loo, A. Lowery, N. Halas, J. West, R. Drezek, Inmunotargeted nanoshells for integrated cancer imaging and therapy, Nano Lett. 5 (4) (2005) 709–711. https://doi10.1021/nl050127s.

[4] S. Lal, P.K. Clare, N.J. Halas, Nanoshell-enabled photothermal cancer therapy: impeding clinical impact, Acc. Chem. Med. Sci. 23 (2008) 217–228. https://doi.org/10.1021/ar800150g.

[5] X. Huang, P.K. Jain, I.H. El-Sayed, M.A. El-Sayed, Plasmonic photothermla therapy using gold nanoparticles, Lasers Med. Sci. 23 (2008) 217–228. https://doi10.1007/s10103-007-0470-x.

[6] T. Niidome, M. Yamagata, Y. Okamoto, Y. Akiyama, H. Takahashi, T. Kawano, Y. Katayama, Y. Niidome, PEG-modified gold nanaorods with a stealth character for *in vivo* applications, J. Control. Release 114 (2006) 343–347. https://doi10.1016/j.jconrel.2006.06.017.

[7] N.S. Abadeer, C.J. Murphy, Recent progress in cancer thermal therapy using gld nanoparticles, J. Phys. Chem. C 120 (2016) 4691–4716. https://doi:10.1021/acs.jpcc.5b11232.

[8] N. Zamora-Romero, V. Robles, C. Alvarez, N. Cuando-Espitia, L.F. Devia-Cruz, E. Penilla, D.L. Halaney, G. Aguilar, Laser-excited gold nanoparticles for treatment of cancer cells in vitro. Medical Laser Applications and Laser-Tissue Interactions VIII, in: L. Lilge (Ed.), SPIE Proceedings, vol. 10417, 2017, p. 1041707. https://doi.org/10.1117/12.2286005.

[9] F. Zhou, D. Xing, Z. Ou, B. Wu, D.E. Resaco, W.R. Chen, Cancer photothermal therapy in the near-infrared region by using single wall carbon nanotubes, J. Biomed. Opt. 14 (2) (2009), 021009. https://doi10.1117/1.3078803.

[10] M.S. Mohamed, A.C. Poulose, S. Veeranarayanan, R.R. Aburto, T. Mitchman, Y. Susuky, Y. Sakamoto, P.M. Ajayan, R.R. Bouchard, Y. Yoshida, T. Maekawa, D. S. Kumar, Plasmonic Fluorescence CdSe/Cu_2 S Hybrid Nanocrystals for Multichannel Imaging and Cancer Directed Photo-Thermal Therapy, vol.14, 2009, 021009, 2, https://doi.org/10.1039/c5nr05225d.

[11] X. Song, H. Gong, S. Yin, L. Cheng, C. Wang, Z. Li, Y. Li, X. Wang, Z. Liu, Ultra-small Iron oxide doped polypyrrole nanoparticles for in vivo multimodal guided photothermal therapy, Adv. Funct. Mater. 24 (2014) 1194–1201. https://doi.org/10.1002/adfm.201302463.

[12] I. Alves de Castro, R. Datta, J. Ou, A. Castellanos-Gomez, S. Sriram, T. Daeneke, K. Kalantar-zadeh, Molybdenum oxides – from fundamentals to functionality, Adv. Mater. 29 (2017) 1701619. https://doi:10.1002/adma.201701619.

[13] T. Pham, P. Nguyen, T. Vo, H. Nguyen, C. Luu, Facile method for synthesis of nanosized β–MoO3 and their catalytic behavior for selective oxidation of methanol to formaldehyde, Adv. Nat. Sci. Nanosci. Nanotechnol. 6 (2015), 045010 6, https://doi:10.1088/2043-6262/6/4/045010.

[14] M.A. Camacho-López, L. Escobar-Alarcón, M. Picquart, R. Arroyo, G. Córdoba, E. Haro-Poniatowski, Micro-Raman study of the m-MoO2 to a-MoO3 transformation induced by cw-laser irradiation, Opt. Mater. 33 (2011) 480–484. https://doi.org/10.1016/j.optmat.2010.10.028.

[15] M. Cano-Lara, S. Camacho-López, A. Esparza-García, M.A. Camacho-López, Laser-induced molybdenum oxide formation by low energy (nJ)–high repetition rate (MHz) femtosecond pulses, Opt. Mater. 33 (2011) 1648–1653. https://doi.org/10.1016/j.optmat.2011.04.029.

[16] S.H. Lee, H. Nishi, T. Tatsuma, Tunable plasmon resonance of molybdenum oxide nanoparticles synthesized in non-aqueous media, Chem. Commun. 53 (2017) 12680–12683. https://doi10.1039/C7CC08090E.

[17] D. Ding, W. Guo, C. Guo, J. Sun, N. Zheng, F. Wang, M. Yan, S. Liu, MoO3-x quantum dots for photoacoustic imaging guided photothermal/photodynamic cancer treatment, Nanoscale 9 (2017) 2020–2029. https://doi10.1039/C6NR09046J.

[18] J. Shi, Y. Kuwahara, M. Wen, M. Navlani-García, K. Mori, T. An, H. Yamashita, Room-temperature and aqueous-phase synthesis of plasmonic molybdenum oxide nanoparticles for visible-light-enhanced hydrogen generation, Chem. Asian J. 00 (2016), 0–0, https://doi:10.1002/asia.201600771.

[19] Y. Yang, Y. Yang, S. Chen, Q. Lu, L. Song, Y. Wei, X. Wang, Atomic-level molybdenum oxide nanorings with full-spectrum absorption and photoresponsive properties, Nat. Commun. 8 (2017) 1559. https://doi10.1038/s41467-017-00850.

[20] Anh Tran T1, K. Krishnamoorthy, Y.W. Song, S.K. Cho, S.J. Kim, Toxicity of nano molybdenum trioxide toward invasive breast cancer cells, ACS Appl. Mater. Interfaces 64 (2014) 2980–2986. https://doi10.1021/am405586d.

[21] W. Yin, T. Bao, X. Zhang, Q. Gao, J. Yu, X. Dong, L. Yang, Z. Gu, Y. Zhao, Biodegradable MoO_x nanoparticles with efficient near-infrared phtothermal and photodynamic therapy at the second biological window, Nanoscale 10 (2018) 1517. https://doi10.1039/C7NR07927C.

[22] W. Liu, X. Li, W. Li, Q. Zahng, H. Bai, J. Li, G. Xi, Highly stable molybdenum dioxide nanoparticles with strong plasmon resonance are promising in photothermal cancer therapy, Biomaterials 163 (2018) 43–54. https://doi10.1016/j.biomaterials.2018.02.021.

[23] Y. Zhan, Y. Liu, H. Zu, Y. Guo, S. Wu, H. Yang, Z. Liu, B. Lei, J. Zhuang, X. Zhang, D. Huang, C. Hu, Phase-controlled synthesis of molybdenum oxide nanoparticles for surface enhanced Raman scattering and photothermal therapy, Nanoscale 10 (2018) 5997–6004. https://doi.org/10.1039/C8NR00413G.

[24] G.1 Song, J. Shen, F. Jiang, R. Hu, W. Li, L. An, R. Zou, Z. Chen, Z. Qin, J. Hu, Hydrophilic molybdenum oxide nanomaterials with controlled morphology and strong plasmonic absorption for photothermal ablation of cancer cells, ACS Appl. Mater. Interfaces 6 6 (2014) 3915–3922. https://doi:10.1021/am4050184.

[25] J. Dowden, The Theory of Laser Materials Processing, first ed., Springer series in materials science, 2008.

[26] D. Zhang, B. Gökce, S. Barcikowski, Laser synthesis and processing of colloids: fundamentals and applications, Chem. Rev. 1175 (2017) 3990–4103. https://doi.org/10.1021/acs.chemrev.6b00468.

[27] S.I. Dolgaev, A.V. Simakin, V.V. Voronov, G.A. Shafeev, F. Bozon-Verduraz, Nanoparticles produced by laser ablation of solids in liquid environment, Appl. Surf. Sci. 186 (2002) 546. https://doi:10.1016/s0169-4332(01)00634-1.

[28] H. Zeng, X.D. Du, S.C. Singh, S.A. Kulinich, S. Yang, J. He, W. Cai, Nanomaterials via laser ablation/irradiation in liquid: a review, Adv. Funct. Mater. 22 (2012) 1333–1353. https://doi:10.1002/adfm.201102295.

[29] M. Madrigal-Camacho, A.R. Vilchis-Nestor, M. Camacho-Lopez, M.A. Camacho-Lopez, Synthesis of MoC@Graphite NPs by short and ultra-short pulses laser ablation in toluene under N_2 atmosphere, Diam. Relat. Mater. 82 (2018) 63–69. https://doi.org/10.1016/j.diamond.2017.12.019.

[30] N. Zamora-Romero, M.A. Camacho-Lopez, M. Camacho-Lopez, A.R. Vilchis-Nestor, V. H Castrejon-Sanchez, S. Camacho-Lopez, G. Aguilar, Molybdenum nanoparticles by pulsed laser ablation and effects of oxidation due to aging, J. Alloy. Comp. 788 (2019) 666–671. https://doi.org/10.1016/j.jallcom.2019.02.270.

[31] G. Marzun, A. Levish, V. Mackert, T. Kallio, S. Barcikowski, P. Wagener, Laser synthesis, structure and chemical properties of colloidal nickel-molybdenum nanoparticles for the substitution of noble metals in heterogeneous catalysis, J. Colloid Interface Sci. (2016). https://doi.org/10.1016/j.jcis. 2016.09.014.

[32] M. Maaza, B.D. Ngom, S. Khamlich, Valency control in MoO3−δ nanoparticles generated by pulsed laser liquid solid interaction, J. Nanoparticle Res. 14 (2012) 714. https://doi.org/10.1007/s11051-011-0714-3.

[33] S. Spadaro1, M. Bonsignore, E. Fazio, F. Cimino, A. Speciale, D. Trombetta, F. Barreca, A. Saija, F. Neri, Molybdenum oxide nanocolloids prepared by an external sield-assisted laser ablation in water, EPJ Web Conf. 167 (2018), 04009. https://doi.org/10.1051/epjconf/201816704009.

[34] V. Amendola, M. Meneghetti, What controls the composition and the structure of nanomaterials generated by laser ablation in liquid solution? Phys. Chem. Chem. Phys. 15 (2013) 3027–3046. https://doi10.1039/C2CP42895D.

[35] V. Amendola, M. Meneghetti, Laser ablation synthesis in solution and size manipulation of noble metal nanoparticles, Phys. Chem. Chem. Phys. 11 (2009) 3805–3821. https://doi.org/10.1039/B900654K.

[36]] S.I. Dolgaev, A.V. Simakin, V.V. Voronov, G.A. Shafeev, F. Bozon-Verduraz, Nanoparticles produced by laser ablation of solids in liquid environment, Appl. Surf. Sci. 186 (2002) 546. https://doi:10.1016/s0169-4332(01)00634-1.

[37] A. Ayi, A.A. Chinyere, K. Varsha, On the synthesis of molybdenum nanoparticles under reducing conditions in ionic liquids, J. Mater. 372716 (2015) 1–7. http://doi.org/10.1155/2015/372716.

[38] N. Khlebtsov, V. Bogatyrev, L. Dykman, A. Melnikov, Spectral extinction of colloidal gold and its biospecific conjugates, J. Colloid Interface Sci. 180 (2) (1996) 436–445, 25, https://doi.org/10.1006/jcis.1996.0323.

[39] J.S. Duque, B.M. Madrigal, H. Riascos, Y.P. Avila, Colloidal metal oxide nanoparticles prepared by laser ablation technique and their antibacterial test, Colloids. Interfaces 3 (2019) 25. https://doi:10.3390/colloids3010025.

[40] M. Shkir, V. Ganesh, I.S. Yahia, et al., J. Mater. Sci. Mater. Electron. 29 (2018) 15838. https://doi.org/10.1007/s10854-018-9670-3.

[41] S. Sun, X. Yang, Y. Zhang, F. Zhang, J. Ding, J. Bao, C. Gao, Enhanced photocatalytic activity of sponge-like ZnFe2O4 synthesized by solution combustion method, Prog. Nat. Sci. 22 (2012) 639–643. https://doi.org/10.1016/j.pnsc.2012.11.008.

[42] T. Theivasanthi, M. Alagar, Lead nanopowder as advanced semi-conductor, An Insight. Res. Appl. Mater 1 (2013) 36–43. https://doi10.12966/ram.07.02.2013.

[43] S. Akbar, H. Baset, Size measurement of metal and semiconductor nanoparticles via uv-vis absorptionspectra, Dig. J. Nanomater. Biostruct. 6 (2011) 709–716.

[44] A. Takami, H. Kurita, S. Koda, Laser-induced size reduction of noble metal particles, J. Phys. Chem. 1038 (1999) 1226–1232. https://doi.org/10.1021/jp983503o.

[45] Peter Strasser, Shirlaine Koh, Toyli Anniyev, Jeff Greeley, Karren More, Chengfei Yu, Zengcai Liu, Sarp Kaya, Dennis Nordlund, Hirohito Ogasawara, Michael F. Toney, Anders Nilsson, Lattice-strain control of the activity in dealloyed core–shell fuel cell catalysts, Nat. Chem. 2 (2010) 454–460. https://doi.org/10.1038/nchem.623.

[46] G. Yang, D. Chen, L. Pengmei, X. Kong, Y. Sun, Z. Wang, Z. Yuan, H. Liu, J. Yang, Core-shell Au-Pd nanoparticles as cathode catalysts for microbial fuel cell applications, Sci. Rep. 6 (2016) 35252. https://doi.org/10.1038/srep35252.

[47] L. Seguin, Infrared and Raman spectra of MoO_3 molybdenum trioxides and $MoO_3 \cdot xH_2O$ molybdenum trioxides hydrates, Spectrochim. Acta 51 (1995) 1323–1344. https://doi.org/10.1016/0584-8539(94)00247-9.

[48] M.A. Camacho-López, E. Haro-Poniatowski, L. Lartundo-Rojas, J. Livaged, M. Juliene, "Amorphous–crystalline transition studied in hydrated MoO_3", Mater. Sci. Eng. 135 (2) (2006) 88–94, 25, https://doi.org/10.1016/j.mseb.2006.08.041.

[49] E. Haro-Poniatowski, C. Julien, B. Pecquenard, J. Livage, Laser-induced structural transformations in MoO3 investigated by Raman spectroscopy, 13, 1998, pp. 1033–1037, 4, https://doi.org/10.1557/JMR.1998.0144.